Modulation Strategies for Anisotropy-Based Position Estimation of PMSMs Using the Neutral Point Voltage

KLAUS SCHUHMACHER[ID], STEPHAN KLEEN[ID], CHRIS MAY[ID], AND MATTHIAS NIENHAUS[ID]

Laboratory of Actuation Technology, Saarland University, 66123 Saarbrücken, Germany

Corresponding author: Klaus Schuhmacher (schuhmacher@lat.uni-saarland.de)

ABSTRACT Information obtained about magnetic anisotropy via neutral point voltage measurements can be used to estimate the position of synchronous and induction machines at all speeds including standstill. Due to its usually high signal-to-noise ratio, this estimation method can be an attractive alternative to approaches that acquire anisotropy information via current measurements. The position estimation method looked at in this paper relies on anisotropy information in the form of position-dependent inductance ratios. These are obtained through measurement of the voltage between the machine's neutral point and an artificial neutral point during the application of different voltage vectors via a two-level switching inverter. We analyze the conditions placed on and the consequences of implementing necessary modifications to a standard space vector modulation. Five different modified modulation strategies are compared and investigated, including two newly proposed strategies which use only a minimal set of active and zero voltage vectors for measurement of the inductance ratios and therefore allow high utilization of available voltage and a high update rate of the estimated position. Experimental results for three low-power three-phase permanent magnet synchronous machines are presented which suggest that modulation strategies that use active measurement vectors in all three instead of only two axes of the machine are less susceptible to systematic deviations in the position estimation that presumably result from nonlinear machine properties. As part of the machine model, a normalizing inductance variation ratio is introduced, which simplifies expressions and supports the comparison of motors.

INDEX TERMS Magnetic anisotropy, neutral point, permanent magnet machines, pulse width modulation, sensorless control, space vector modulation, star point, zero-sequence voltage.

I. INTRODUCTION

Estimating position and speed of synchronous and inductance machines from electrical quantities instead of using mechanical sensors offers opportunities to save space and cost and to increase reliability. The use of magnetic anisotropies has been strongly investigated over the past three decades in order to complement methods based on induced voltages and allow estimation at very low speeds and standstill. While the voltage induced by rotor movement is proportional to speed, estimation via magnetic anisotropy is based on machine inductances varying with position. The nonlinear properties of the iron core and varying magnetic circuits in the machine are the cause for their position dependency.

To acquire information related to the position dependent machine inductances, the machine phases must be excited with AC signals such as sinusoidal or pulsed signals. In three-phase permanent magnet synchronous machines (PMSMs), this excitation can be applied either in the stationary or estimated rotating frame of the machine. There exists a wide variety of approaches to exploit the anisotropy information using different forms of excitation, measurement, signal processing and methods to determine position and speed [1], [2]. In this paper, we focus only on estimation approaches that use the discrete voltage vectors from a two-level switching inverter as the source of excitation to obtain information

The associate editor coordinating the review of this manuscript and approving it for publication was Feifei Bu[ID].

about the varying inductances in the machine. The following advantages can be identified: applying pulses with the highest available voltage in the system, the DC link voltage, results in very high transient excitation and therefore maximizes the response [3]; also, such an approach offers the possibility of direct calculation without feedback path and therefore has no theoretical limit in estimation bandwidth, only in sampling rate. Therefore, there is potential to achieve high-performance control.

The majority of anisotropy-based approaches are based on current measurements [4], the first one being the INFORM technique proposed by Schroedl [5], [6]. Since current sensors are anyway needed for field-oriented control, no additional hardware is needed in this case. When injecting voltages and evaluating current changes dependent on the varying inductances, measurement noise however poses an important factor to be considered. Especially when using the time derivative for direct calculation it can quickly become a problem. The noise makes high bandwidth estimation with no or little filtering difficult, especially when also trying to inject as small additional voltage signals as possible. One solution for this problem was presented in [7] and consists of the use of fast ADCs and oversampling, estimating the current derivative via linear regression.

An interesting alternative however can be to use the zero-sequence voltage that can be acquired from the voltage at the machine's neutral point, which must be accessible in this case. Variants of this latter approach were proposed in [3], [8] and [9] for induction machines and in [10]–[16] for PMSMs. Due to its low noise content this approach can provide position estimation with high signal-to-noise ratio with relatively low hardware and computational requirements and will be the focus of this paper. Analytical comparisons between the anisotropy information provided via current or current derivative measurements and zero-sequence voltage measurements can be found in [14], [15].

As we will see, modifications to conventional space vector modulation (SVM) are necessary in order to successfully employ position estimation based on zero-sequence voltage measurements and discrete voltage vector excitation. In previous works, different modifications of the SVM have been used, but these have often been described in little detail or only under certain conditions such as low speed and low voltage. Concerning investigations into voltage utilization in terms of achievable voltage vector amplitudes and other effects of choosing a certain kind of modified SVM, only limited information can be found in [14]. The aim of this work is therefore to analyze the requirements placed on modified SVM strategies and compare different approaches. As part of this we will review modified SVM strategies that have been proposed in the literature and propose two new ones that use a minimal set of voltage vectors. Key aspects of this investigation are differences in the achievable voltage vector amplitude and in estimation results, where the latter will be investigated by experiments on three low-power PMSMs.

II. ESTIMATION PRINCIPLE

The estimation principle that is used in this paper is outlined in two steps. In the first step, a simplified machine model in matrix form is introduced which neglects saturation and hysteresis effects and allows the flux linkages to be represented as a linear superposition of the flux linkages produced by the permanent magnets and the windings. It is shown that the anisotropy information from which the machine position is determined is contained in inductance ratios that can be identified by means of measurements taken at the neutral point. In the second step, the calculation of the estimated position from the inductance ratios is derived based on a common assumption of the inductance matrix's position dependency.

A. ELECTRICAL MACHINE MODEL

In this section, a simplified electrical model of a three-phase star-connected permanent magnet synchronous machine will be derived in stationary coordinates. In order to represent the equations, two different coordinate systems will be used: first, the *abc* frame, which is directly related to the three physical machine phases and the voltage vectors that can be applied using a three-phase inverter; second, the $\alpha\beta0$ frame with its orthogonal axes α and β and the zero-sequence axis, which yields simpler equations and has no linear dependence between its components. The $\alpha\beta0$ frame also allows for a better comparison with approaches that inject voltage signals and measure currents, as these are typically modelled in $\alpha\beta$ or in the rotating frame *dq*. The zero-sequence axis is typically not considered there because it has no influence on the phase currents. Vectors in the *abc* frame will be displayed with the superscript "p" for "physical", while vectors in $\alpha\beta0$ will use the commonly used superscript "s" for "stator". If no superscript is used for vectors or matrices, the equation is true for both stationary reference frames. Voltages u, currents i and flux linkages Ψ are transformed from one frame to the other via the amplitude invariant Clarke transform $\boldsymbol{T}_{\mathrm{C}}$:

$$\boldsymbol{x}^{\mathrm{s}} = \boldsymbol{T}_{\mathrm{C}}\boldsymbol{x}^{\mathrm{p}}, \tag{1}$$

$$\boldsymbol{x}^{\mathrm{p}} = \boldsymbol{T}_{\mathrm{C}}^{-1}\boldsymbol{x}^{\mathrm{s}}, \tag{2}$$

where

$$\boldsymbol{T}_{\mathrm{C}} = \frac{2}{3}\begin{bmatrix} 1 & -1/2 & -1/2 \\ 0 & \sqrt{3}/2 & -\sqrt{3}/2 \\ 1/2 & 1/2 & 1/2 \end{bmatrix} \tag{3}$$

and

$$\boldsymbol{x}^{\mathrm{s}} = \begin{bmatrix} x_{\alpha} & x_{\beta} & x_0 \end{bmatrix}^{\mathrm{T}}, \tag{4}$$

$$\boldsymbol{x}^{\mathrm{p}} = \begin{bmatrix} x_{\mathrm{a}} & x_{\mathrm{b}} & x_{\mathrm{c}} \end{bmatrix}^{\mathrm{T}}, \tag{5}$$

$$x \in \{u, i, \Psi\}. \tag{6}$$

The electrical machine model in either of the stationary frames is expressed as

$$\boldsymbol{u} = \boldsymbol{R}\boldsymbol{i} + \frac{\mathrm{d}}{\mathrm{d}t}\boldsymbol{\Psi}, \tag{7}$$
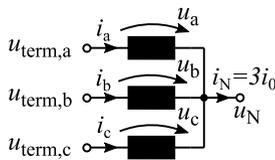
FIGURE 1. Three phases of an electrical machine in star connection.

where $\boldsymbol{u}$ is the vector of phase voltages, $\boldsymbol{i}$ is the vector of phase currents and $\boldsymbol{\Psi}$ is the vector of the total flux linkages associated with the phases. $\boldsymbol{R}$ is the resistance matrix. To enable an understanding of the principle of neutral point based position estimation, the total flux linkage vector is assumed to be the superposition of the permanent magnet flux linkage vector and the stator flux linkage vector

$$\boldsymbol{\Psi} = \boldsymbol{\Psi}_{\text{PM}}(\varphi) + \boldsymbol{\Psi}_{\text{s}} \qquad (8)$$

$$= \boldsymbol{\Psi}_{\text{PM}}(\varphi) + \boldsymbol{L}(\varphi)\boldsymbol{i}, \qquad (9)$$

where $\boldsymbol{L}$ is the inductance matrix that is dependent on the electrical rotor position φ due to the magnetic anisotropy. $\boldsymbol{\Psi}_{\text{PM}}$ is also position dependent, because it is aligned with the permanent magnets on the rotor. However, hysteretic effects are not considered and there is assumed to be no dependency of $\boldsymbol{L}$ and $\boldsymbol{\Psi}_{\text{PM}}$ on the stator current. The inductance matrix in *abc* is further assumed to be symmetrical and invertible, defined by

$$\boldsymbol{L}^{\text{p}}(\varphi) = \boldsymbol{L}^{\text{p}} = \begin{bmatrix} L_{\text{aa}} & L_{\text{ab}} & L_{\text{ca}} \\ L_{\text{ab}} & L_{\text{bb}} & L_{\text{bc}} \\ L_{\text{ca}} & L_{\text{bc}} & L_{\text{cc}} \end{bmatrix}, \qquad (10)$$

whereas in $\alpha\beta0$, the inductance matrix can be derived as

$$\boldsymbol{L}^{\text{s}} = \boldsymbol{T}_{\text{C}}\boldsymbol{L}^{\text{p}}\boldsymbol{T}_{\text{C}}^{-1} = \begin{bmatrix} L_{\alpha\alpha} & L_{\alpha\beta} & 2L_{0\alpha} \\ L_{\alpha\beta} & L_{\beta\beta} & 2L_{0\beta} \\ L_{0\alpha} & L_{0\beta} & 2L_{00} \end{bmatrix}. \qquad (11)$$

Using (9), (7) can be rewritten as

$$\boldsymbol{u} = \boldsymbol{R}\boldsymbol{i} + \left(\frac{\text{d}}{\text{d}t}\boldsymbol{L}\right) \cdot \boldsymbol{i} + \boldsymbol{L} \cdot \left(\frac{\text{d}}{\text{d}t}\boldsymbol{i}\right) + \frac{\text{d}}{\text{d}t}\boldsymbol{\Psi}_{\text{PM}}. \qquad (12)$$

The phase voltages are the difference between the voltages applied at the machine terminals and the neutral point

$$\boldsymbol{u}^{\text{p}} = \boldsymbol{u}_{\text{term}}^{\text{p}} - u_{\text{N}}\begin{bmatrix} 1 & 1 & 1 \end{bmatrix}^{\text{T}}, \qquad (13)$$

$$\boldsymbol{u}^{\text{s}} = \boldsymbol{u}_{\text{term}}^{\text{s}} - u_{\text{N}}\begin{bmatrix} 0 & 0 & 1 \end{bmatrix}^{\text{T}}, \qquad (14)$$

as depicted in Fig. 1, where $u_{\text{term},\lambda}$, $\lambda \in \{a, b, c\}$ and u_{N} are the respective voltages with respect to the common inverter ground. Under the assumption that $i_0 = 0$ and $\text{d}i_0/\text{d}t = 0$, the neutral point voltage can then be expressed as

$$u_{\text{N}} = \left(\begin{bmatrix} 0 & 0 & 1 \end{bmatrix}\boldsymbol{L}^{\text{s}^{-1}}\begin{bmatrix} 0 \\ 0 \\ 1 \end{bmatrix}\right)^{-1}\begin{bmatrix} 0 & 0 & 1 \end{bmatrix}\boldsymbol{L}^{\text{s}^{-1}}$$

$$\cdot \left(\boldsymbol{u}_{\text{term}}^{\text{s}} - \boldsymbol{u}_{\text{slow}}^{\text{s}}\right) \qquad (15)$$

$$= \boldsymbol{\kappa}^{\text{s}}\left(\boldsymbol{u}_{\text{term}}^{\text{s}} - \boldsymbol{u}_{\text{slow}}^{\text{s}}\right), \qquad (16)$$

with

$$\boldsymbol{\kappa}_{\text{s}} = \begin{bmatrix} \kappa_\alpha & \kappa_\beta & 1 \end{bmatrix}, \qquad (17)$$

$$\kappa_\alpha = \frac{-L_{\beta\beta}L_{0\alpha} + L_{\alpha\beta}L_{0\beta}}{L_{\alpha\alpha}L_{\beta\beta} - L_{\alpha\beta}^2} = \frac{Y_{0\alpha}}{Y_{00}}, \qquad (18)$$

$$\kappa_\beta = \frac{-L_{\alpha\alpha}L_{0\beta} + L_{\alpha\beta}L_{0\alpha}}{L_{\alpha\alpha}L_{\beta\beta} - L_{\alpha\beta}^2} = \frac{Y_{0\beta}}{Y_{00}}, \qquad (19)$$

$$\boldsymbol{u}_{\text{slow}}^{\text{s}} = \boldsymbol{R}^{\text{s}}\boldsymbol{i}^{\text{s}} + \left(\frac{\text{d}}{\text{d}t}\boldsymbol{L}^{\text{s}}\right) \cdot \boldsymbol{i}^{\text{s}} + \frac{\text{d}}{\text{d}t}\boldsymbol{\Psi}_{\text{PM}}^{\text{s}} \qquad (20)$$

$$= \boldsymbol{R}^{\text{s}}\boldsymbol{i}^{\text{s}} + \omega \cdot \left(\frac{\partial}{\partial\varphi}\boldsymbol{L}^{\text{s}}\right) \cdot \boldsymbol{i}^{\text{s}} + \omega \cdot \frac{\partial}{\partial\varphi}\boldsymbol{\Psi}_{\text{PM}}^{\text{s}} \qquad (21)$$

and

$$\omega = \frac{\text{d}\varphi}{\text{d}t}, \qquad (22)$$

as has been shown in [15]. Analogously to (11), Y_{ij} are the entries of the inverse of the inductance matrix

$$\boldsymbol{Y}^{\text{s}} = \boldsymbol{L}^{\text{s}^{-1}}, \qquad (23)$$

giving additional insight into the meaning of these inductance ratios. According to (15)-(17), the neutral point voltage depends therefore on the inductance ratios κ_α and κ_β, on the applied terminal voltages and on the slowly changing part $\boldsymbol{u}_{\text{slow}}$, consisting of resistive voltage drops and voltage induced due to rotor movement. These terms can be considered constant within a small time period that is much smaller than the machine's electrical time constant as well as the time for one electrical revolution. Furthermore, it can be observed that κ_α and κ_β are position dependent, whereas κ_0 is equal to one and therefore contains no position information. By analogously subtracting the voltage of an artificial neutral point, which connects three equal resistors leading to the machine terminals and can be expressed as

$$u_{\text{AN}} = \begin{bmatrix} 1 & 1 & 1 \end{bmatrix}\boldsymbol{u}_{\text{term}}^{\text{p}} = \begin{bmatrix} 0 & 0 & 1 \end{bmatrix}\boldsymbol{u}_{\text{term}}^{\text{s}} \qquad (24)$$

$$= u_{\text{term},0}, \qquad (25)$$

the zero-sequence component of $\boldsymbol{u}_{\text{term}}^{\text{s}}$ is removed, leading to

$$u_{\text{NAN}} = u_{\text{N}} - u_{\text{AN}} \qquad (26)$$

$$= \begin{bmatrix} \kappa_\alpha & \kappa_\beta & 1 \end{bmatrix}\left(\boldsymbol{u}_{\text{term}}^{\text{s}} - \boldsymbol{u}_{\text{slow}}^{\text{s}}\right) - u_{\text{term},0} \qquad (27)$$

$$= \begin{bmatrix} \kappa_\alpha & \kappa_\beta & 0 \end{bmatrix}\boldsymbol{u}_{\text{term}}^{\text{s}} - \begin{bmatrix} \kappa_\alpha & \kappa_\beta & 1 \end{bmatrix}\boldsymbol{u}_{\text{slow}}^{\text{s}}. \qquad (28)$$

To complete the picture, it is worth mentioning that

$$u_{\text{NAN}} = -u_0. \qquad (29)$$

In [9], the voltages between machine terminals and the neutral point were measured and summed instead, which is a different measurement approach but provides the same information. The slowly changing part $\boldsymbol{u}_{\text{slow}}$ can be considered a disturbance signal, which becomes more significant as speed increases. By applying two different voltage vectors whose difference is $\Delta\boldsymbol{u}_{\text{term}}$ in close succession and evaluating only the differences in u_{NAN} between these vectors, $\boldsymbol{u}_{\text{slow}}$ remains almost unchanged and is therefore eliminated. This then allows a precise measurement of the inductance ratios up to high speeds and rejection of possible resistive

imbalances, leaving only

$$\Delta u_{\text{NAN}} = -\Delta u_0 = \begin{bmatrix} \kappa_\alpha & \kappa_\beta & 0 \end{bmatrix} \Delta \boldsymbol{u}_{\text{term}}^{\text{s}} \qquad (30)$$

or

$$\Delta u_{\text{NAN}} = -\Delta u_0 = \begin{bmatrix} \kappa_\text{a} & \kappa_\text{b} & \kappa_\text{c} \end{bmatrix} \Delta \boldsymbol{u}_{\text{term}}^{\text{p}} \qquad (31)$$

respectively, where

$$\kappa_\text{a} + \kappa_\text{b} + \kappa_\text{c} = 1. \qquad (32)$$

These final equations show the relationship between the difference of two applied voltage vectors, the inductance ratio vector $\boldsymbol{\kappa}$ and Δu_{NAN}. $\boldsymbol{\kappa}$ contains two-dimensional anisotropy information that can be used to estimate the motor position via direct calculation. Δu_{NAN} can be interpreted as a *zero-sequence anisotropy voltage*.

B. POSITION ESTIMATION

As the next step, it is necessary to discuss how the position information can be obtained from the vector of inductance ratios $\boldsymbol{\kappa}$. We therefore assume a diagonal matrix $\boldsymbol{L}^{\text{p}}$ that consists of an isotropic part and an anisotropic part. The isotropic part is constant and is comprised of the mean inductance L_Σ multiplied with the identity matrix $\boldsymbol{I}$. The entries in the anisotropic part vary sinusoidally with the amplitude $2L_\Delta$ and with twice the frequency of the electrical rotor position so that

$$\boldsymbol{L}^{\text{p}} = L_\Sigma \boldsymbol{I} + 2L_\Delta$$
$$\cdot \begin{bmatrix} \cos(2\varphi) & 0 & 0 \\ 0 & \cos\left(2\left(\varphi - \dfrac{2\pi}{3}\right)\right) & 0 \\ 0 & 0 & \cos\left(2\left(\varphi - \dfrac{4\pi}{3}\right)\right) \end{bmatrix}. \qquad (33)$$

As we have seen in (15-19), anisotropy information in neutral point based approaches expresses itself in the form of inductance ratios and not in absolute values of inductances or their reciprocals as is the case with approaches based on current measurements, which has also been discussed in [14] and [15]. For this reason we define an *inductance variation ratio*

$$r = L_\Delta / L_\Sigma. \qquad (34)$$

Representing the normalized induction variation by this ratio will significantly contribute to the simplification of the equations, the understanding of the general dependencies and the comparability between machines.

Accordingly, (33) can be rewritten as

$$\boldsymbol{L}^{\text{p}} = L_\Sigma \boldsymbol{I} + 2L_\Sigma r$$
$$\cdot \begin{bmatrix} \cos(2\varphi) & 0 & 0 \\ 0 & \cos\left(2\left(\varphi - \dfrac{2\pi}{3}\right)\right) & 0 \\ 0 & 0 & \cos\left(2\left(\varphi - \dfrac{4\pi}{3}\right)\right) \end{bmatrix}. \qquad (35)$$

and the inductance matrix and the inductance ratio vector in $\alpha\beta0$ are obtained as

$$\boldsymbol{L}^{\text{s}} = L_\Sigma \boldsymbol{I} + L_\Sigma r \begin{bmatrix} \cos(2\varphi) & \sin(2\varphi) & 2\cos(2\varphi) \\ \sin(2\varphi) & -\cos(2\varphi) & -2\sin(2\varphi) \\ \cos(2\varphi) & -\sin(2\varphi) & 0 \end{bmatrix} \qquad (36)$$

and

$$\boldsymbol{\kappa}^{\text{s}} = \begin{bmatrix} \kappa_\alpha \\ \kappa_\beta \\ \kappa_0 \end{bmatrix}^{\text{T}} = \frac{1}{1 - r^2} \cdot \begin{bmatrix} -r\cos(-2\varphi) + r^2\cos(4\varphi) \\ -r\sin(-2\varphi) + r^2\sin(4\varphi) \\ 1 - r^2 \end{bmatrix}^{\text{T}}. \qquad (37)$$

In the *abc* frame, the inductance ratios are found to be

$$\boldsymbol{\kappa}^{\text{p}}$$
$$= \begin{bmatrix} \kappa_\text{a} \\ \kappa_\text{b} \\ \kappa_\text{c} \end{bmatrix}^{\text{T}} = \boldsymbol{\kappa}^{\text{s}} \boldsymbol{T}_{\text{C}} = \begin{bmatrix} \dfrac{1}{3} & \dfrac{1}{3} & \dfrac{1}{3} \end{bmatrix} + \frac{1}{3} \frac{1}{(1 - r^2)}$$
$$\cdot \begin{bmatrix} -2r\cos(2\varphi) + 2r^2\cos(4\varphi) \\ -2r\cos\left(2\left(\varphi - \dfrac{2\pi}{3}\right)\right) + 2r^2\cos\left(4\left(\varphi - \dfrac{2\pi}{3}\right)\right) \\ -2r\cos\left(2\left(\varphi - \dfrac{4\pi}{3}\right)\right) + 2r^2\cos\left(4\left(\varphi - \dfrac{4\pi}{3}\right)\right) \end{bmatrix}^{\text{T}}. \qquad (38)$$

Consequently, the assumptions made about the inductance matrix result in inductance ratios that contain a fourth harmonic, which would cause harmonics in the estimated position when using a direct calculation approach via the *arctangent* function.

In [11] an interesting find was made, which has received little attention so far. It was shown that purely sinusoidal inductance ratio signals can be obtained by a nonlinear transformation, effectively removing the influence of the fourth harmonic. Based on this we define another row vector of inductance ratios

$$\boldsymbol{\rho}^{\text{s}} = \frac{1}{\sqrt{3}} \begin{bmatrix} \sqrt{\kappa_\text{b}\kappa_\text{c}/\kappa_\text{a}} \\ \sqrt{\kappa_\text{a}\kappa_\text{c}/\kappa_\text{b}} \\ \sqrt{\kappa_\text{a}\kappa_\text{b}/\kappa_\text{c}} \end{bmatrix}^{\text{T}} \boldsymbol{T}_{\text{C}}^{-1}, \qquad (39)$$

which compared to [11] was only scaled by $1/\sqrt{3}$ to allow for better comparison with $\boldsymbol{\kappa}^{\text{s}}$. Together with (38) this leads to

$$\boldsymbol{\rho}^{\text{s}} = \frac{1}{\sqrt{1 - r^2}} \begin{bmatrix} r\cos(-2\varphi) \\ r\sin(-2\varphi) \\ 1 \end{bmatrix}^{\text{T}}. \qquad (40)$$

By applying the *arctangent* function, the position can clearly be derived correctly, requiring no knowledge of r except of its sign. A negative r corresponds with $L_{\text{dd}} < L_{\text{qq}}$ when the inductance matrix is transformed to the *dq0* frame. Since the *arctangent* function returns only values between
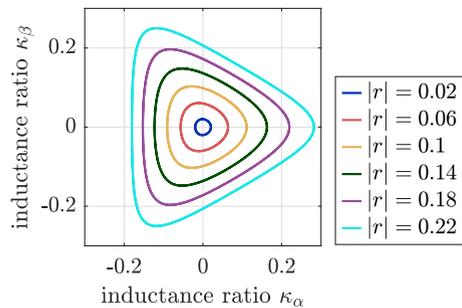
FIGURE 2. Loci of the inductance ratio vector κ in the $\alpha\beta$-plane for different absolute values of the inductance variation ratio $|r|$. The 4th harmonic causes deviations from circular shape with increasing $|r|$.

FIGURE 3. Loci of the inductance ratio vector ρ in the $\alpha\beta$-plane for different absolute values of the inductance variation ratio $|r|$. The shape remains circular regardless of $|r|$.

TABLE 1. Discrete voltage vectors applicable via a three-phase two-level switching inverter with DC link voltage u_{DC}.

| | $\boldsymbol{u}_{\text{term}}^{\text{p}}$ | | | $\boldsymbol{u}_{\text{term}}^{\text{s}}$ | | |
	a	b	c	α	β	0
$\boldsymbol{u}_0$	0	0	0	0	0	0
$\boldsymbol{u}_1$ (+a)	u_{DC}	0	0	$2/3u_{DC}$	0	$1/3u_{DC}$
$\boldsymbol{u}_2$ (-c)	u_{DC}	u_{DC}	0	$1/3u_{DC}$	$1/\sqrt{3}u_{DC}$	$2/3u_{DC}$
$\boldsymbol{u}_3$ (+b)	0	u_{DC}	0	$-1/3u_{DC}$	$1/\sqrt{3}u_{DC}$	$1/3u_{DC}$
$\boldsymbol{u}_4$ (-a)	0	u_{DC}	u_{DC}	$-2/3u_{DC}$	0	$2/3u_{DC}$
$\boldsymbol{u}_5$ (+c)	0	0	u_{DC}	$-1/3u_{DC}$	$-1/\sqrt{3}u_{DC}$	$1/3u_{DC}$
$\boldsymbol{u}_6$ (-b)	u_{DC}	0	u_{DC}	$1/3u_{DC}$	$-1/\sqrt{3}u_{DC}$	$2/3u_{DC}$
$\boldsymbol{u}_7$	u_{DC}	u_{DC}	u_{DC}	0	0	u_{DC}

arrangement or the nonlinear behaviour of the soft-magnetic material, in particular saturation effects [1]. Such deviations can be modelled as (current-dependent) harmonics, phase shifts or offsets that may require identification and adequate compensation.

Information about possible compensation structures can be found for example in [17] and [18] and is not further discussed here. For the motors used in this work, a compensation of harmonic components is not necessarily required to achieve sufficiently accurate position estimation. Only a relatively simple correction function for current-dependent offsets in the estimated position will therefore be described and used in the experimental investigation in section IV.

III. SPACE VECTOR MODULATION
A. STANDARD SVM
Typically, modern electrical drives use two-level three-phase switching inverters to apply voltages to the machine phases that have previously been calculated by the control algorithm, which is most often a field-oriented control. If exactly one switch is always conducting in every leg of the inverter, eight discrete voltage vectors are possible for $\boldsymbol{u}_{\text{term}}$ according to Table 1, where u_{DC} is the voltage of the DC link. $\boldsymbol{u}_0$ and $\boldsymbol{u}_7$ are so-called *zero vectors*, whereas the others are usually referred to as *active vectors* [19].

In order to apply arbitrary voltage vectors, modulation strategies are necessary which synthesize this so-called reference vector as a time-average of the discrete voltage vectors over one modulation period. Space vector modulation (SVM) can be considered the conventional approach to generate the pulsed voltage waveforms which are applied to the inverter switches. Even though, technically, all such approaches use a modulation of space vectors, the term SVM is typically used for a specific implementation that uses the two active vectors closest to the reference vector and the two zero vectors [19]. Such an approach keeps the current ripple small and we will refer to this as *standard SVM*. The two zero vectors are redundant and represent an additional degree of freedom which can for example be used to minimize losses in the switching devices [20]. Fig. 4 shows an example of a reference vector $\boldsymbol{u}_r$ that is synthesized using the active vectors $\boldsymbol{u}_1$ (+a) and $\boldsymbol{u}_2$ (-c), whose shares of the PWM period are $k_1 = T_{\text{u1}}/T_{\text{PWM}}$ and $k_2 = T_{\text{u2}}/T_{\text{PWM}}$. The zero vectors are applied during the

$-\pi/2$ and $+\pi/2$, the *atan2* function should be used for implementation, leading to

$$\varphi = \begin{cases} -\dfrac{1}{2}\,\text{atan2}\left(\rho_\beta, \rho_\alpha\right) - \dfrac{\pi}{2} + k\pi, & r < 0 \\[2mm] -\dfrac{1}{2}\,\text{atan2}\left(\rho_\beta, \rho_\alpha\right) + k\pi, & r > 0 \end{cases}, \quad (41)$$

where $k \in \mathbb{N}$. As with all anisotropy-based approaches, the estimated position has an uncertainty of 180° electrical. This uncertainty must be resolved by an initial polarity detection procedure, which can for example be found in [5], [11] and [13]. It is worth mentioning that an equivalent position can also be obtained by a method shown in [13], which skips the intermediate step of creating purely sinusoidal signals and does not involve calculating square roots and divisions. The expected loci of κ^{s} and ρ^{s} for the assumed inductance matrix are shown in Figs. 2 and 3 for a range of values of $|r|$, clearly revealing the disturbing influence of the fourth harmonic of the electrical rotor position in κ^{s} with increasing $|r|$.

The simplified model together with the transformation in (39) leads to an "ideal anisotropy vector" that has a constant length and rotates with -2φ without additional harmonics. This idealized representation enables parameterless position estimation requiring no additional knowledge of the machine except the mentioned sign of the inductance variation as long as the model describes the machine sufficiently well. The components of the anisotropy vector in real machines can however deviate from this ideal description for various reasons, including the motor geometry, the winding

FIGURE 4. Example of a reference vector u_r synthesized via standard SVM. The reference vector is the time-average of the discrete voltage vectors over one modulation period.

remaining time so that

$$T_{\text{PWM}} = T_{\text{u}1} + T_{\text{u}2} + T_{\text{u}0} + T_{\text{u}7}. \tag{42}$$

B. REQUIREMENTS FOR NEUTRAL POINT BASED POSITION ESTIMATION

Here, we will discuss the requirements placed on modulation strategies implementing the neutral point based approach being pursued in this paper. We will first keep the considerations on an abstract level to make generally valid statements before practical implementation is discussed in sections III-C and III-D. It is first explained that at least three suitable voltage vectors are required to perform the measurements of u_{NAN} that are necessary for position estimation. We will refer to such vectors as *measurement vectors*. Three reasons that lead to a minimum time requirement for these vectors are then mentioned. It is shown that these minimum times are not adhered to in certain voltage regions of a standard SVM so that modifications are necessary. The limitations on the achievable voltage amplitude associated with these modifications are discussed and a theoretical limit is given for a best-case consideration. Then, desirable characteristics of a suitable modified modulation strategy are listed before three known and two newly proposed modulation strategies are presented and compared in the sections that follow.

Concerning the requirement for a certain number and orientation of voltage vectors, equation (30) has shown that Δu_{NAN} depends only on κ_α and κ_β and the differential voltage vector applied at the machine terminals. More precisely, (30) is a single linear equation with the two unknowns κ_α and κ_β which are required for the position estimation approach being discussed here. In order to determine both and directly calculate the rotor position, it is therefore necessary to apply at least two Δu_{term} in linearly independent directions in the $\alpha\beta$-plane, requiring at least three suitable voltage vectors.

In order to take useful measurements of u_{NAN}, the corresponding voltage vectors must be applied for a minimum time duration due to three reasons. The first reason is the transient response occurring at the neutral point after a switching event. As the measurements in Fig. 5 show, the inductances and parasitic capacitances in a machine and its cables typically create significant overshoot and ringing at the neutral point.
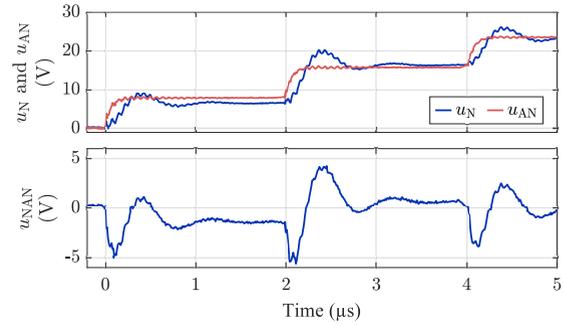
FIGURE 5. Measured data of u_N, u_{AN} and resulting u_{NAN} acquired from motor M1 during operation. u_N and u_{AN} were analogously lowpass filtered with time constant $\tau \approx 46.6$ ns.
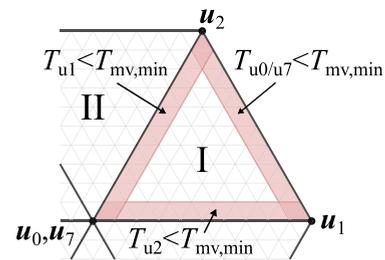
FIGURE 6. Red areas show voltage regions where estimation is not possible when using standard SVM in sector I.

Even more pronounced overshoot and ringing was reported in [21]. Consequentially, measurements right after switching would be distorted and must therefore be avoided. Secondly, the A/D converter also needs a minimum time to sample the voltage. And finally, inverter dead-times must also be considered because they influence the effective switching instants depending on the phase currents. All of these factors result in the requirement for a minimum time $T_{\text{mv,min}}$, for which each of the measurement vectors must be applied so that $T_{\text{mv}} \geq T_{\text{mv,min}}$.

If standard SVM is used, there are regions in the hexagon of applicable voltage vectors, where this requirement for minimum times would not be fulfilled. This is illustrated in Fig. 6 for one of the six voltage sectors. At the two borders to neighboring sectors, the time for which the more distant of the two active voltage vectors is applied becomes too small. In the high voltage region located at the outer border, the same is true for the zero voltage vectors. As a result of this, the position estimation would not be possible in these areas. It therefore becomes apparent that modified modulation strategies are necessary when using a neutral-point based approach as described before.

The standard SVM can be modified for example by extending the duration of existing discrete voltage vectors or substituting vectors, which however leads to a reduction in achievable voltage amplitude. We will now look at the maximum voltage that can be applied with a suitably modified modulation strategy. We define an estimation period T_{est}
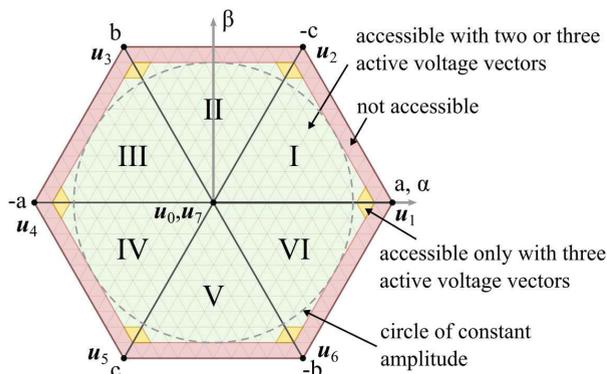
FIGURE 7. Theoretical maximum voltage range with modified modulation strategies due to the requirement of minimum time for suitable switching states, shown for $T_{\mathrm{mv,min}}/T_{\mathrm{est}} = 0.1$.

corresponding to the time required to update the position estimation. This will typically be equal to one or multiple PWM periods. Because at least three different voltage vectors are needed for the estimation as discussed before, the accessible voltage region is reduced at the outer border as shown in Fig. 7. To describe the reduction in voltage amplitude, a comparison can be drawn between the amplitude $\hat{u} = |\boldsymbol{u}_{\mathrm{term}}^{\mathrm{s}}|$ achievable with a modified SVM and the one achievable with standard SVM. A voltage reduction factor k_{red} is therefore defined, where

$$\hat{u}_{\mathrm{max,modified}} = (1 - k_{\mathrm{red}})\,\hat{u}_{\mathrm{max,standard}} \quad (43)$$

$$= (1 - k_{\mathrm{red}})\,\frac{1}{\sqrt{3}}u_{\mathrm{DC}}. \quad (44)$$

In the best case the voltage reduction factor is

$$k_{\mathrm{red,min}} = \frac{1 \cdot T_{\mathrm{mv,min}}}{T_{\mathrm{est}}} \quad (45)$$

compared to standard SVM. This is because in addition to the two adjacent active voltage vectors, at least one zero vector or one additional active voltage vector must be applied for $T_{\mathrm{mv,min}}$ in every estimation period, which does not contribute in the direction of the reference vector. Therefore, this is to be considered the theoretical minimum; the actual reduction depends however on the specific modified SVM approach, as will be further discussed.

There is another noteworthy aspect. The yellow edge regions in Fig. 7 are only accessible if the three active voltage vectors closest to these regions are used for measurement. If $T_{\mathrm{mv}}/T_{\mathrm{est}}$ is greater than a certain threshold or if overmodulation is desired, the use of these vectors becomes therefore necessary to avoid a further reduction in voltage amplitude. This threshold is given by

$$T_{\mathrm{mv}}/T_{\mathrm{est}} = \frac{1 - \cos(30°)}{2 - \cos(30°)} = \frac{1 - \sqrt{3}/2}{2 - \sqrt{3}/2} \approx 0.118 \quad (46)$$

and can be geometrically derived as the ratio where the yellow regions touch the circle of constant amplitude. For

the sake of simplicity, it is assumed here that this threshold is not exceeded and that no overmodulation is used. For the further investigation, it is also assumed that the modified SVM is used repeatedly in all PWM periods. The achievable voltage amplitude would otherwise differ between periods, which will probably be undesirable in most cases.

How should a modified modulation strategy be designed? There are in fact diverse possibilities in realizing suitable modified SVM strategies. The following are a few characteristics that an ideal modified SVM approach and the measurement approach that is inherently connected with it should fulfill:

- high update rate of the anisotropy information
- high voltage utilization
- high rejection of systematic errors such as
  - -- varying common modes of u_{N} and u_{AN} causing errors due to common mode gain in subtraction
  - -- errors due to non-linear machine behaviour
  - -- low-frequency part $\boldsymbol{u}_{\mathrm{slow}}$
- low complexity of implementation, i.e.
  - -- low computational effort
  - -- low hardware capability requirements
- low additional current ripple to avoid audible noise and torque ripple
- few or no additional switching events

It is probably not surprising, that these goals cannot all be optimally satisfied at the same time and that compromises have to be made. Some of these aspects are also difficult to compare, for example the complexity of implementation, which depends strongly on the hardware that is being used. However, we will try to cover as many aspects as possible when presenting different possible approaches.

C. MODIFIED SVM STRATEGIES USED IN PREVIOUS WORKS

For neutral point based position estimation, a few modified modulation strategies have been published so far. All of these strategies implement measurement vectors that fulfill the minimal time requirement to estimate the position independently of the reference voltage vector. However, differences between modification strategies have not yet been investigated in detail. For example, the varying levels of reduction of the achievable voltage amplitude remained largely unmentioned, which is certainly due to many works focusing only on the low speed range. Also, the effects that choosing a certain modified SVM has on the measurement of the inductance ratios and therefore also on the position estimation have not yet been analyzed.

In [9], one of the earliest works, it was proposed to add one active measurement vector at the end of one PWM period and compensate for this with the opposite vector at the beginning of the next PWM period, making measurements during both vectors as shown in Fig. 8(a). For direct calculation of the position, this procedure must be carried out in at least two
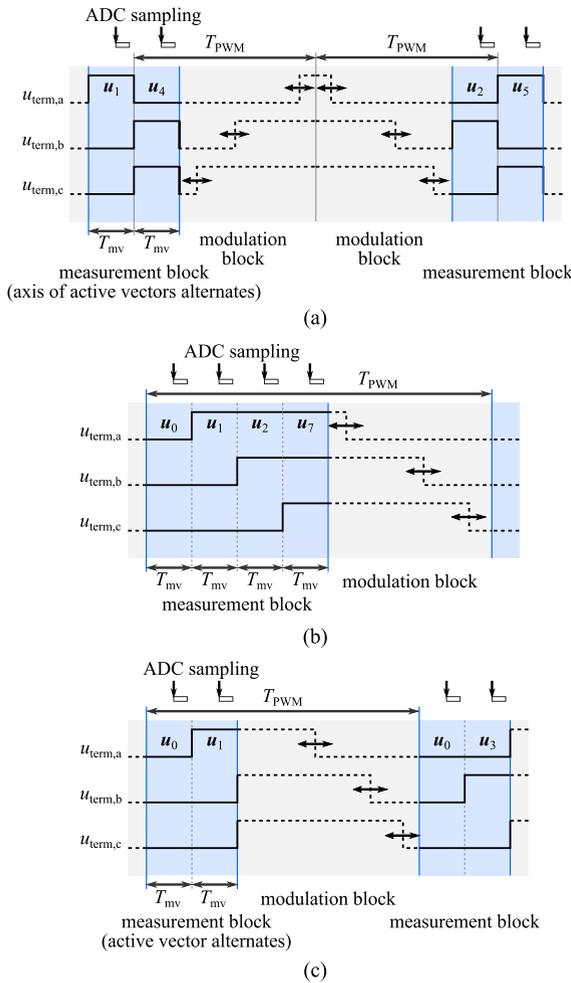
FIGURE 8. Illustration of modified SVM approaches that were used in previous works. Differences are found mainly in the measurement block: (a) using opposing active vectors in alternating axes [9]; (b) using two zero vectors and two neighboring active vectors [16] and (c) using one zero vector and one active vector in alternating axes [11].

but preferably in all three axes. In the latter case six PWM periods are required so that $T_{\text{est}} = 6T_{\text{PWM}}$, however the position can be updated every two PWM periods when a new pair of measurements becomes available. Advantages of this approach can be identified as follows. Due to the use of opposing voltage vectors, the maximum realizable magnitude of Δu_{term} is applied and thus a high signal-to-noise ratio is obtained. Since the vectors are applied directly after each other, they compensate each other almost immediately. Additionally, the mirrored neighboring modulation blocks result in a behavior similar to center-aligned PWMs, which is typically preferred due to lower harmonic distortion compared to edge-aligned pulses [22]. Presumably the main downside of this approach occurs during high speed operation, since the measurements of u_{NAN} are spread over multiple PWM periods during which the rotor position can change considerably. The voltage reduction factor is

$$k_{\text{red}} = \frac{6T_{\text{mv}}}{6T_{\text{PWM}}} = \frac{1 T_{\text{mv}}}{T_{\text{PWM}}}, \tag{47}$$

which means that high voltage amplitudes can be achieved, but this comes at the cost of a relatively long estimation period.

In [16] a different approach was used. The beginning of each PWM period was kept fixed and started with a zero vector, then the phases were quickly switched one after the other. Four measurements were taken during the resulting two zero and two active vectors as shown in Fig. 8(b). The measurement vectors are compensated for in the modulation block by shifting the edges by the same amount as in the measurement block. This has the advantage that all measurements needed to acquire the inductance ratio vectors are performed within one single block and at every PWM period. However, it also leads to a substantial reduction in voltage with

$$k_{\text{red}} = \frac{6T_{\text{mv}}}{T_{\text{PWM}}}, \tag{48}$$

because the order of the pulse edges is not chosen in dependence of the SVM sector. The limiting factor is the achievable amplitude in the sector that is on the opposite side of the measurement vectors. In the case illustrated, this would be sector IV.

Another modified strategy has been proposed in [11] and spreads the measurements over three PWM periods, where each period starts with a zero vector and then one phase is switched, where the latter is alternated each PWM period, as shown in Fig. 8(c). Measurements are taken at the zero vector and the following active vector, leading to a total of six measurements over three PWM periods. The voltage reduction depends on whether the measurement vectors are compensated for in the modulation block of the respective PWM period. If this is the case, the voltage reduction is

$$k_{\text{red}} = \frac{9T_{\text{mv}}}{3T_{\text{PWM}}} = \frac{3T_{\text{mv}}}{T_{\text{PWM}}}, \tag{49}$$

otherwise it is

$$k_{\text{red}} = \frac{6T_{\text{mv}}}{3T_{\text{PWM}}} = \frac{2T_{\text{mv}}}{T_{\text{PWM}}}. \tag{50}$$

In the second case, the active measurement vectors compensate each other over three PWM periods. A noteworthy downside of this modified SVM is that it produces significant current ripple and therefore potentially audible noise at $f_{\text{PWM}}/3$ and multiples of it due to the alternating vectors in the measurement block, which are not immediately compensated for. Also, very high speed operation can become an issue again because the measurements are spread over three PWM periods.

In all of the discussed approaches, at least two measurements of u_{NAN} are always performed in close succession. This ensures a proper elimination of the low frequency part u_{slow}. Additionally, the measurements are also performed at fixed time instants, which simplifies triggering of the ADC and allows calculating the position at regular intervals without delay.

In [12], the authors proposed to shift the pulses of a standard SVM to guarantee minimum measurement vector

times. If applied to edge-aligned PWM, it would be similar to the approach shown in Fig. 8(c). However, the underlying estimation principle was slightly different from the one described in this paper since it did not make use of differential measurements to eliminate u_{slow}, focusing mainly on low-speed operation.

As an alternative for cases where the modulator does not provide enough flexibility to modify the SVM as described above, estimation can also be realized by inserting additional standard SVM periods solely for excitation and measurement purposes between those that apply the voltage vector requested by the control algorithm [14]. However, this then leads to stronger limitations either in voltage utilization or in the update rate of the position, depending on how often these periods are inserted. For this reason, this approach is not further pursued here.

D. NOVEL MODIFIED SVM STRATEGIES WITH MINIMAL NUMBER OF MEASUREMENT VECTORS

The approaches that were discussed in the last section use either four or six measurement vectors per estimation period to acquire the desired anisotropy information. Adding to the existing approaches we want to propose two new modified SVM strategies which use only the minimum number of three measurement vectors to acquire the inductance ratios per estimation period. Within the first new strategy, measurement is accomplished using the two active vectors that are naturally used in standard SVM per each sector plus one zero vector. In this way the highest possible voltage amplitudes can be achieved with

$$k_{\text{red}} = \frac{1 T_{\text{mv}}}{T_{\text{PWM}}} \qquad (51)$$

and the position can be estimated at each PWM period. The SVM is therefore modified similarly to the one shown in Fig. 8(b), however the active vectors depend on the SVM sector and the fourth measurement is omitted as can be seen in Fig. 9(a). In order to prevent high-frequency switching between vectors it is advisable to implement a hysteresis logic when determining which measurement vectors to use.

The second proposed strategy uses one active vector in each of the three axes, resulting in a zero vector on average. The modulation block is similar to that in Fig. 8(a), resulting in center-aligned pulses and an update of the position with every second PWM period. One unique advantage of this strategy is also that all measurements are performed at the same common mode voltage $u_{\text{term},0}$, therefore making it less susceptible to systematic common mode errors. The implementation of this modulation strategy can be somewhat more complex compared to the other strategies because some PWM periods require three edges to be generated. The voltage reduction factor for this strategy is

$$k_{\text{red}} = \frac{3 T_{\text{mv}}}{2 T_{\text{PWM}}} = \frac{\frac{3}{2} T_{\text{mv}}}{T_{\text{PWM}}}. \qquad (52)$$

Table 2 sums up some of the relevant properties of the five modified SVM strategies presented. Abbreviations are

(a)

(b)
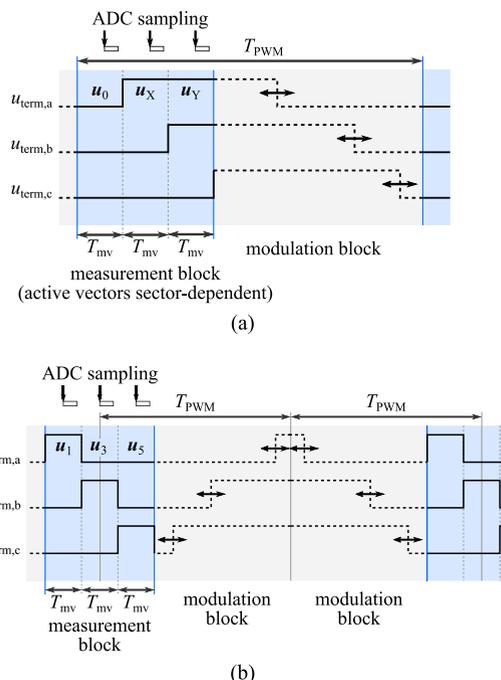
FIGURE 9. Novel modified SVM approaches with minimal number of measurement vectors: (a) using sector-dependent active measurement vectors and (b) using active measurement vectors in all three axes.

TABLE 2. Overview of the five modified SVM (mSVM) strategies under investigation.

Abbreviation	mSVM1	mSVM2	mSVM3	mSVM4	mSVM5
Figure	Fig. 8(a)	Fig. 8(b)	Fig. 8(c)	Fig. 9(a)	Fig. 9(b)
Reference	[9]	[16]	[11]	-	-
$T_{\text{est}}/T_{\text{PWM}}$	6	1	3	1	2
Voltage reduction factor k_{red} in $T_{\text{mv}}/T_{\text{est}}$	6	6	6 or 9[a]	1	3
Voltage reduction factor k_{red} in $T_{\text{mv}}/T_{\text{PWM}}$	1	6	2 or 3[a]	1	1.5
Measurement vectors per T_{est}	6	4	6	3	3
Nr. of axes with active measurement vectors	3	2	3	2	3
Alignment in the modulation blocks	center	edge	edge	edge	center
Measurements split into multiple measurement blocks	yes	no	yes	no	no

[a] depending on compensation, see text

given to each of the five *modified SVM* (mSVM) strategies, enabling clear correlation with the experimental results.

IV. EXPERIMENTAL INVESTIGATION

A. EXPERIMENTAL SETUP

To obtain experimental results, the three low-power PMSMs listed in Table 3 were analyzed under application of the various modulation strategies. While M2 and M3 are commercially available motors, M1 is a prototype motor that was designed for anisotropy-based sensorless operation in a conveyor roller. In the case of M2, the neutral point was made accessible by the manufacturer, whereas in the case of M3, the neutral point is accessible by default, which is quite rare.

TABLE 3. Parameters of motors under investigation.

Motor	M1	M2	M3
Nominal voltage	24 V	24 V	9 V
Nominal power	70 W	100 W	3 W
Phase resistance R	1.1 Ω	0.37 Ω	4.7 Ω
Mean inductance L_Σ	0.435 mH	0.332 mH	0.65 mH
Inductance variation ratio $r = L_\Delta / L_\Sigma$ (at zero current)	−0.121	−0.036	−0.023
Permanent magnet flux linkage Ψ_{PM}	9.89 mVs	3.11 mVs	1.21 mVs
Nr. of pole pairs	8	7	4

M1: prototype conveyor roller motor
M2: Faulhaber 4221G024BXTR
M3: maxon EC 20 flat 9V sensorless
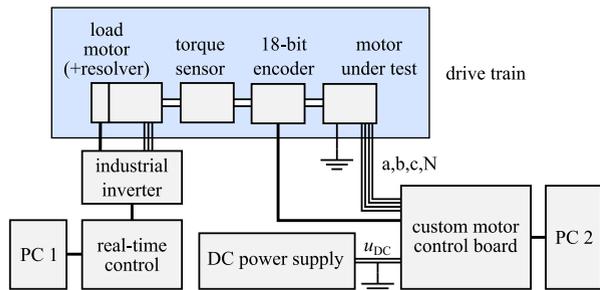
FIGURE 10. Schematic overall view of the experimental setup used in this work.
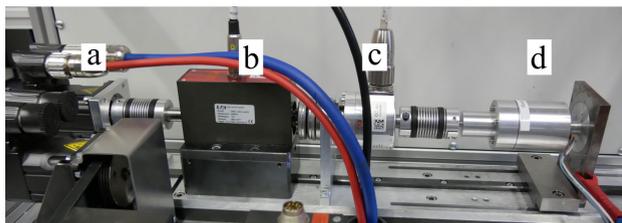
FIGURE 11. Drive train as part of the experimental setup with motor M1 mounted: (a) load motor, (b) torque sensor, (c) reference position sensor and (d) motor under test.

The principal experimental setup is shown in Fig. 10. Unless stated otherwise, the motors under test are coupled to a drive train consisting of a load motor, a torque sensor and an 18-bit optical encoder with an accuracy of ±0.1° that served as a position reference as depicted in Fig. 11. Torque measurements were used only for validation and are not shown in this work. The housing of the motor is connected to the negative rail of the DC power supply to prevent external disturbances from coupling onto the neutral point over parasitic capacitances in the motor. The load motor is given references from a PC using a real-time control and is controlled either to constant speed or constant load torque.

In all of the experiments the same custom motor control board shown in Fig. 12 is used to control the motor under test, perform measurements of u_{NAN} and the phase currents and read the 18-bit encoder. The usage of a custom control board offers the flexibility that is necessary to realize the
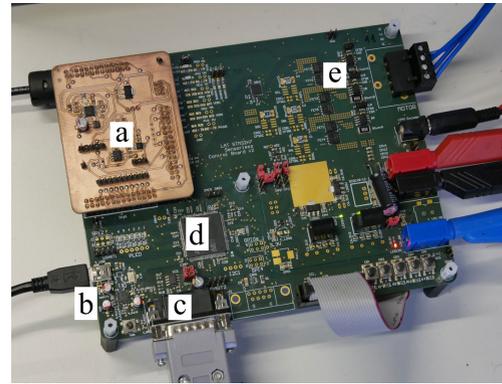
FIGURE 12. Custom motor control board as part of the experimental setup: (a) u_{NAN} subtractor circuit, (b) USB interface, (c) position sensor interface, (d) STM32H753xx microcontroller and (e) inverter and shunt current sensors.

different modified modulation strategies and allows for precise triggering of the measurements in synchronization with the PWM. It essentially consists of an STM32H753xx microcontroller that runs at 400 MHz and has an internal 16-bit ADC, a MOSFET based inverter, three shunt-based current sensors and an SPI-to-USB interface to transfer measured data to a second PC. The neutral point and artificial neutral point voltages are scaled down on the board using resistive voltage dividers and lowpass filtered with a very small time constant of $\tau \approx 46.6$ ns. They are then passed to an add-on board which includes three fast operational amplifiers, of which two serve as voltage followers for u_N and u_{AN} and one as a subtractor to obtain u_{NAN}. The embedded software running on the microcontroller was written in *C*.

The PWM frequency was chosen to be 32 kHz for motors M1 and M2 and 64 kHz for motor M3, considering its smaller electrical time constants. Choosing a lower PWM frequency can result in audible noise, reduces the sampling rate and increases the achievable voltage amplitude but provides very similar position estimation results as confirmed in experiments on motors M1 and M2 at 10 kHz PWM frequency. For the sake of simplicity, a constant-torque-angle strategy with $i_d^{ref} = 0$ was used in the field-oriented control for all measurements. The duration for the measurement vectors was set to $T_{mv} = 2$ μs for all motors. All tests were conducted with the DC link voltage at nominal level.

The model derived in section II does not include any dependency of the inductance ratios on the stator currents. In order to address offsets under load, a correction function was used that considers the measured currents in the estimated d- and q-axes of the machine. It is based on the correction function proposed in [6] and is described by

$$\varphi = \tilde{\varphi} - k_{corr} \arctan\left(\frac{i_q L_{qq}}{i_d L_{dd} + \Psi_{PM}}\right), \qquad (53)$$

where $\tilde{\varphi}$ is the raw position resulting from the estimation approach presented in section II-B. The coefficient k_{corr} was obtained empirically for each motor at low speed operation.
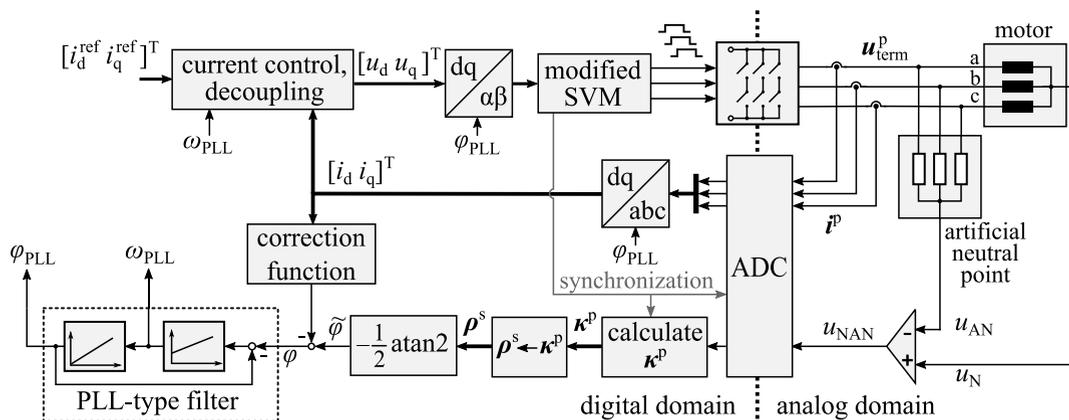
FIGURE 13. Block diagram of the sensorless control scheme used in the experiments. The ADC measurements and the calculation of the inductance ratios are synchronized to the application of the modified SVM. Stator current correction according to (53) and a PLL-type filter are applied to the estimated position. The parameters of the PI controller in parallel form were $k_P = 1014$ and $k_I = 257.06 \cdot 10^3$.

In order to obtain even cleaner position and speed estimates, a PLL-type filter was used which consists of a PI controller and an integrator and was set to a relatively high bandwidth of 200 Hz so that the dynamic performance of the speed control was not limited. Note also that such a structure does not lead to a phase lag at constant speed. Alternatively, the PLL can also be left out and the speed can be calculated by forming the derivative. A block diagram of the overall sensorless control scheme is shown in Fig. 13.

B. EXPERIMENTAL RESULTS

The experimental results are divided into four parts. The first part compares the position estimation results and the underlying inductance ratios for all five modulation strategies at moderate speed and zero current. Both the deviations between estimated and reference positions as well as the inductance ratios indicate differences between those modulation strategies which use measurement vectors in two axes and those which use them in all three axes of the machine. Since the loci of the inductance ratios for the strategies involving two axes deviate from the expected ones, this effect is then further investigated in the second part. Systematic offsets are found which clearly depend on the axes of the measurement vectors. In the third part, results using the two novel modified SVM strategies are shown, demonstrating good position estimation for operation at high speed, high load and high voltage utilization. Finally, results are shown that demonstrate the performance of the estimation technique under transient conditions.

1) COMPARISON OF ALL FIVE MODULATION STRATEGIES AT MODERATE SPEED AND ZERO CURRENT

For a first comparison, only motors M1 and M2 are considered. The load motor drove the motors under test at a speed corresponding to an electrical frequency of 20 Hz, while they were being current controlled to $i_q = 0$ to simulate a no load condition. The estimated position after PLL filtering
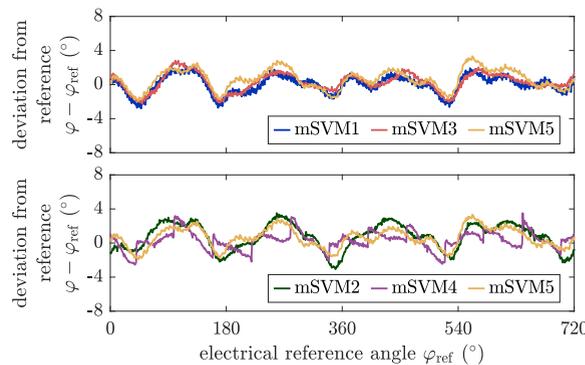
FIGURE 14. Measured deviation from reference position for motor M1 using different modulation strategies at $n = 150$ r/min and current controlled to zero.
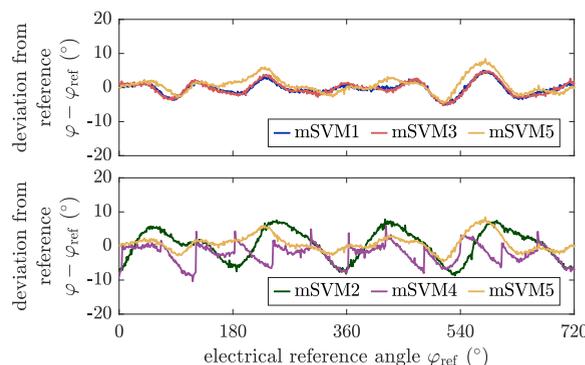
FIGURE 15. Measured deviation from reference position for motor M2 using different modulation strategies at $n = 171.4$ r/min and current controlled to zero.

was used for the field-oriented control. Figs. 14 and 15 show the deviations from the reference position for all of the five applied modulation strategies and both motors. The position information from before the PLL is shown, which is therefore unfiltered. At first glance it is clear that the noise is very small
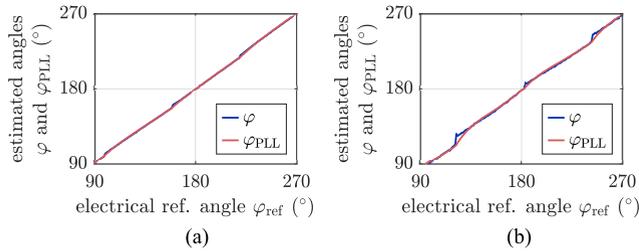
FIGURE 16. Estimated position before and after the PLL affected by discontinuities due to the use of sector-dependent measurement vectors with mSVM4. Graphs show measured data for (a) motor M1 and (b) motor M2.

FIGURE 17. Scatter plots including circle fits of inductance ratio vectors κ and ρ in the $\alpha\beta$-plane for motor M1 at $n = 150$ r/min and current controlled to zero, using mSVM1.

but that there are fluctuations in the estimated positions. The fluctuations were found to be highly repetitive over multiple mechanical revolutions and should therefore not be considered as measurement noise. While for mSVM1, mSVM3 and mSVM5 the curves are highly coincidental, larger differences exist for mSVM2 and mSVM4. In general, higher fluctuations could be observed for motor M2, which may be attributed to the smaller inductance variation ratio. What is particularly noticeable for mSVM4 are the jumps in the deviations that occur roughly every 60°, which correspond to the time instants where the voltage sector changes. Fig. 16 shows this effect on the estimated position before and after filtering with the PLL. These jumps in the estimated position can have a negative impact especially at low speed, when they are large compared to the changes from the actual movement of the rotor. For motor M2, the estimated position in Fig. 15 also exhibits a small offset of a few degrees for mSVM4 compared to the other modulation strategies. It is difficult to draw further conclusions only from the estimated positions, so that further investigations concentrate on the inductance ratios, which are the basis of the calculated positions.

Fig. 17 shows measured data of both inductance ratio vectors κ and ρ for motor M1 as scatter plots. mSVM1 was used in this case. It is important to mention that the plots do not give a correct impression about noise content because data points of multiple mechanical revolutions are included, leading also to multiple revolutions of ρ in the $\alpha\beta$-plane on slightly different paths. Circle fits are also shown, which were calculated afterwards using the Pratt method [23]. One can see that the data points of ρ are much closer to being circular, thereby validating the model used. The centers of both circle fits lie almost exactly at the origin. For motor M1, significant differences were hardly noticeable for any of the other four modulation strategies. However, for motor M2 some differences became visible as is shown for ρ in Fig. 18. Between mSVM1, mSVM3 and mSVM5, no significant difference can be identified. For mSVM4 however, the points seem to be divided into three segments and therefore deviate significantly from the expected circular shape. Besides that, a considerable offset in the $\alpha\beta$-plane can also be noticed for mSVM2. Both modulation strategies are very similar and – differently from the other strategies – use active measurement vectors in only two of the three axes. Thus, it seems plausible,
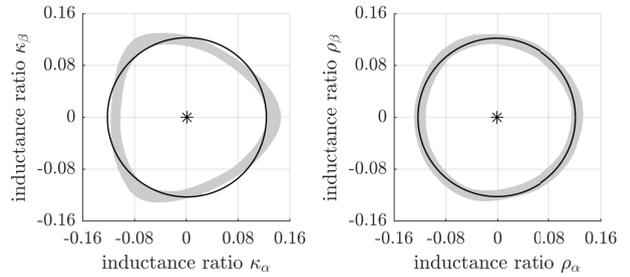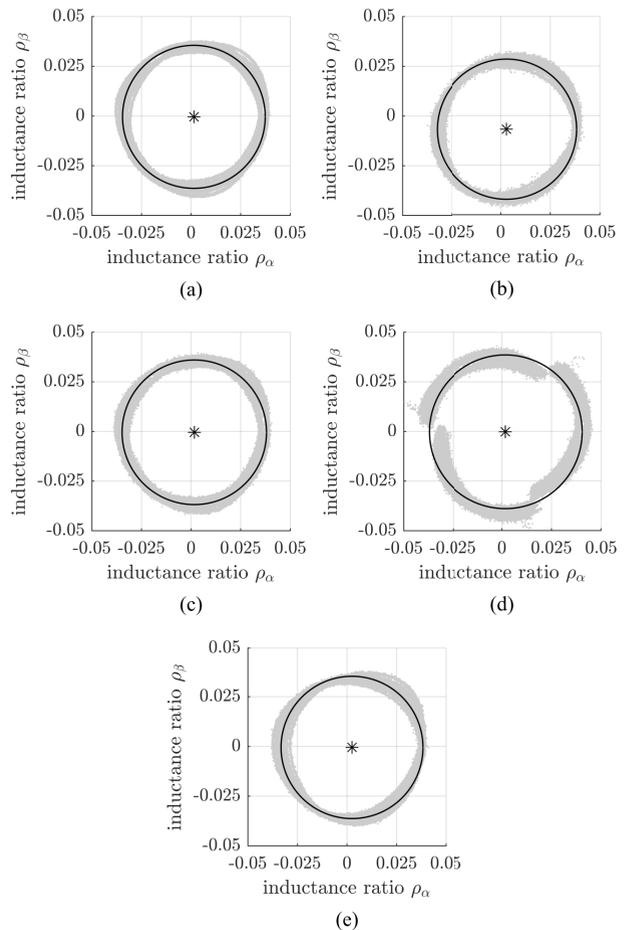
FIGURE 18. Scatter plots including circle fits of inductance ratio vector ρ in the $\alpha\beta$-plane for motor M2 at $n = 171.4$ r/min and current controlled to zero, using different modulation strategies: (a) mSVM1, (b) mSVM2, (c) mSVM3, (d) mSVM4, (e) mSVM5.

that the asymmetry corresponding to the use of measurement vectors in only two axes causes the asymmetries observed in the measurements involving mSMV2 and mSVM4.

2) EFFECT OF ACTIVE MEASUREMENT VECTORS IN ONLY TWO AXES

In order to investigate the effect of using active measurement vectors in two as opposed to in all three axes,
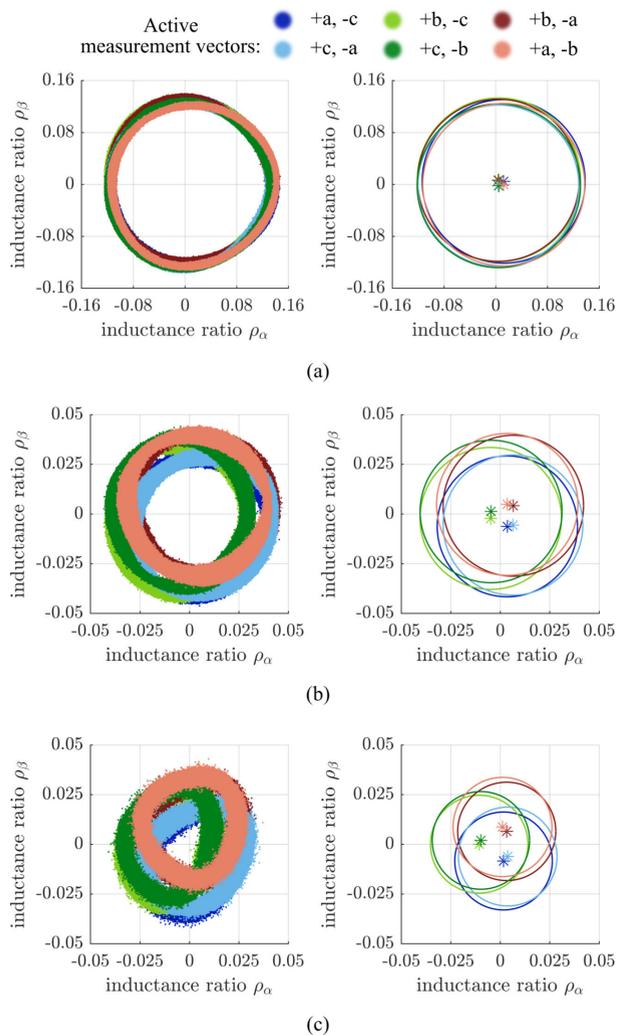
FIGURE 19. Scatter plots (left) and corresponding circle fits (right) of inductance ratio vector ρ in the $\alpha\beta$-plane for (a) motor M1, (b) motor M2 and (c) motor M3, using modulation similar to mSVM4 but with fixed measurement vectors at $n = 1$ r/min and no external load. For motors M2 and M3, the usage of active measurement vectors in only two axes leads to significant offsets.

FIGURE 20. Scatter plot and corresponding circle fit of inductance ratio vector ρ in the $\alpha\beta$-plane for motor M2 when using mSVM1 but discarding the measurements from one of the three axes at $n = 1$ r/min and no external load.

the mSVM4 modulation strategy was applied to all three motors. Here, each pair of active vectors corresponding to the six voltage sectors was held fixed for the duration of a test, instead of being dependent on the voltage sector, thus resulting in continuous plots of the inductance ratios for each vector pair. Because motor M3 was too small to be used on the test bench, all motors were run without test bench in speed control at a very low speed of $n = 1$ r/min and no external load for this test.

The obtained data and calculated circle fits are shown in Fig. 19 for all three motors. For motors M2 and M3, the circle fits and their estimated centers clearly reveal systematic offsets in dependence of the used measurement vectors. This explains very well the behavior that was observed when using mSVM2 and mSVM4 in Fig. 18. However, such a dependence on the used voltage vectors is not compatible with the linear model in equation (30). The effect can also not

be explained by existent, but very small common mode errors that occur in the analog subtraction of u_N and u_{AN}. Instead, this effect reveals the limitations of the simplified model as it seems to come from nonlinear machine properties such as saturation, hysteresis and/or eddy currents combined with the usage of active measurement vectors in only two of the three axes. Using measurement vectors in all three axes instead seems to compensate a large part of the nonlinear behavior so that $\boldsymbol{\rho}$ moves mostly on a circle that has its center in the origin as shown for mSVM1, mSVM3 and mSVM5 in Fig. 18.

This assumption was further verified by using mSVM1 but considering only the measurements from two of the three axes. The effect on the inductance ratios was very similar as can be seen in Fig. 20. Note that only the estimation algorithm but not the modulation itself was changed in this experiment compared to the experiment behind Fig. 18(a). Even though the offsets that were observed are of very systematic nature, eliminating them involves more than just a static offset correction because they have shown to be also dependent on the operating point in further tests. This is therefore not further pursued here.

For motor M1, the effect of using measurement vectors in two versus three axes was much smaller as seen in Fig. 19(a). The reason for this might be the fact that this motor has significantly higher inductance variations so that the impact of the modulation strategy on the measured inductance ratios is small compared to the inherent variations. This would also explain why the effect is smaller for M2 than it is for M3. However, further investigations seem necessary to obtain better understanding of the physical background.

3) RESULTS USING THE NOVEL MODIFIED SVM STRATEGIES AT HIGH SPEED AND HIGH LOAD

Anisotropy-based techniques can be used not only at low speed but also at high speed operation. Especially the two proposed modulation strategies should be well suitable also for high speed operation because they allow both a high utilization of available voltage and also a high update rate of the position. Moreover, the measurements for one position estimation are not split into multiple blocks.
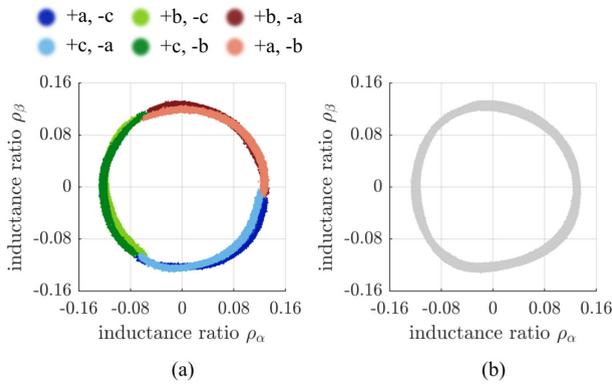
FIGURE 21. Scatter plots of inductance ratio vector ρ for motor M1 at voltage utilization of $\approx 75\%$. The motor was speed controlled to $n = 950$ r/min at constant load torque using different modulation strategies: (a) mSVM4, $i_{q,mean} \approx 1.56$ A and (b) mSVM5, $i_{q,mean} \approx 1.5$ A. For mSVM4, the data points are colored according to the active measurement vectors used.

At $T_{PWM} = 1/(32 \text{ kHz})$ and $T_{mv} = 2$ μs, the voltage reduction factor is $k_{red} = 6.4\%$ for mSVM4 and $k_{red} = 9.6\%$ for mSVM5. In many cases, using the anisotropy based estimation throughout the whole speed range might therefore be a reasonable alternative to switching to an observer or other estimator that uses the induced voltage as a source of information even though a small percentage of the otherwise available voltage is lost due to the modified SVM. This is because it is then unnecessary to design and parameterize the observer and a strategy for smooth transition between low and high speed operation. If algorithms for both the anisotropy-based estimation and the observer need to be executed in parallel during the transition, then more reserves in computational power are also required.

Further tests were therefore conducted on the test bench for motors M1 and M2 at different operating points up to high speed and high current that have confirmed consistently good estimation performance. In the following, results are shown for operating points that utilize approximately 75% of the voltage that would be available with standard SVM. The motors under test were running in speed control and a relatively high constant load torque was applied via the load motor. The speeds were $n = 950$ r/min for motor M1 and $n = 3500$ r/min for motor M2.

Figs. 21 and 23 show the inductance ratios $\boldsymbol{\rho}$ in the $\alpha\beta$-plane that were obtained for motors M1 and M2 when using the two novel modulation strategies. The respective deviations between the estimated positions before and after the PLL and the reference position are shown in Figs. 22 and 24. Similar to the behavior at moderate speed, there are again higher fluctuations in the unfiltered position for motor M2 than for motor M1 and the mean errors vary by a few electrical degrees depending on the modulation strategy, which offers potential for further compensation efforts. For motor M2, there seems to be some impact of the load current on the amplitude and shape of the inductance ratio locus. Overall, the small deviations demonstrate that also at an operating point with high speed and current the position is estimated with good accuracy in field-oriented control.
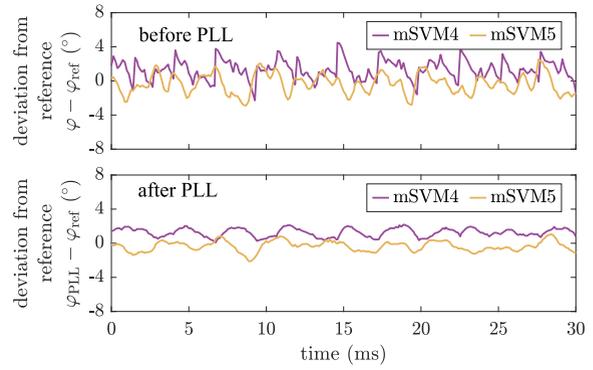
FIGURE 22. Differences between reference position from encoder and estimated position before and after the PLL for motor M1 using mSVM4 and mSVM5 at high speed and constant load torque, $n = 950$ r/min, $i_{q,mean} \approx 1.56$ A (mSVM4) / 1.5 A (mSVM5).
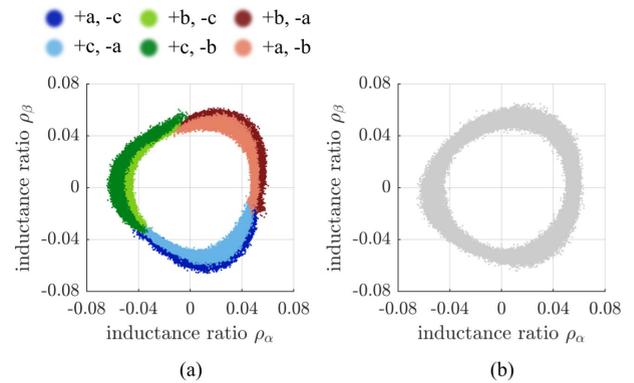
FIGURE 23. Scatter plots of inductance ratio vector ρ for motor M2 at voltage utilization of $\approx 75\%$. The motor was speed controlled to $n = 3500$ r/min at constant load torque using different modulation strategies: (a) mSVM4, $i_{q,mean} \approx 3.04$ A and (b) mSVM5, $i_{q,mean} \approx 2.94$ A. For mSVM4, the data points are colored according to the active measurement vectors used.
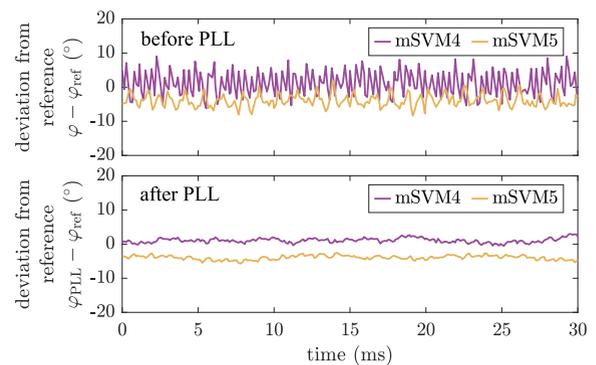
FIGURE 24. Differences between reference position from encoder and estimated position before and after the PLL for motor M2 using mSVM4 and mSVM5 at high speed and constant load torque, $n = 3500$ r/min, $i_{q,mean} \approx 3.04$ A (mSVM4) / 2.94 A (mSVM5).

4) ESTIMATION UNDER TRANSIENT CONDITIONS

Often, estimation performance during transients such as sudden changes in speed or load torque is also of interest. As the raw position $\tilde{\varphi}$ is directly calculated from the inductance ratios via the *arctangent* function, this position is not limited
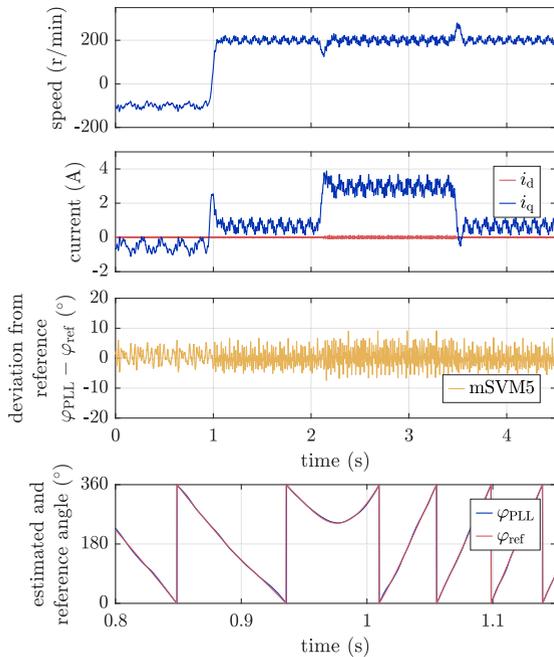
FIGURE 25. Estimation during speed and load transients. Motor M2 is controlled via speed control, using mSVM5. At $t \approx 1$ s, the speed reference is changed stepwise from $n = -100$ r/min to $n = +200$ r/min. From $t \approx 2.1$ s to $t \approx 3.4$ s, a constant load torque is applied via the load motor that causes a current of $i_q \approx 2.95$ A. The bottom diagram shows a close-up of the estimated and reference position during the reversal of direction.

in bandwidth but only in sampling rate. The optional PLL used in this paper adds a dynamic component to the estimation structure, however the high bandwidth of 200 Hz ensures that highly dynamic estimation remains guaranteed. This is possible due to the low amount of noise present in the measurements of the zero-sequence voltage and therefore also in the calculated inductance ratios and position estimates. As demonstrated in Fig. 25 for motor M2 using mSVM5, transient estimation errors in φ_{PLL} accordingly proved to be practically unnoticeable.

V. CONCLUSION

This work showed that modified SVM strategies are necessary when estimating the rotor position from two-dimensional anisotropy information obtained via neutral point voltage measurements. Following a review of existing modified SVM strategies found in the literature two new strategies were proposed that use only a minimal number of voltage vectors for exploiting the anisotropy information in the form of inductance ratios. A detailed analysis of the total of five discussed modulation strategies has been conducted based both on the fundamental design of the modulation periods and on experimental results to point out relevant differences that support the selection of a suitable modulation strategy depending on the specific use case. The differences between the modulation strategies are primarily with respect to the maximum achievable amplitude of the voltage, the robustness against systematic offsets in the inductance ratio vectors and the suitability for high speeds.

Our results show that there can be significant differences in the measured inductance ratio vectors ρ depending on whether active measurement vectors in only two or in all three axes are used in the modified SVM strategy. When active measurement vectors in only two axes were used, systematic offsets in the $\alpha\beta$-plane were observed. This effect can be attributed to nonlinear properties of the machine and differed in intensity for the three PMSMs that were investigated in this work. The use of active measurement vectors in all three axes, in contrast, seems to almost completely compensate the offsets in the $\alpha\beta$-plane. Further research is currently ongoing to gain deeper insight into the physical background of this effect. It is also planned to investigate the effect of modified SVM strategies on the current ripple using spectral analysis, in particular in the context of audible noise.

The two newly proposed modulation strategies allow to both utilize a wide range of the available voltage and estimate the position with a high update rate. One approach (mSVM4) uses one zero vector and the two active vectors that are naturally used in standard SVM. The other new approach (mSVM5) uses three active vectors that are evenly distributed in the $\alpha\beta$-plane. Both were able to estimate the position with high performance for use in field-oriented control at different operating points up to high speed and high current. While mSVM4 allows for the highest voltage utilization and highest update rate, the varying active measurement vectors can result in discontinuous position estimation due to changing offsets in the $\alpha\beta$-plane, which is most noticeable at low speeds. In particular for motors that do not exhibit these offsets to a significant extent such as motor M1 in our investigation, mSVM4 can be a recommendable modulation strategy. The modulation strategy mSVM5, in contrast, is a well-balanced alternative suitable for a wider range of motors, as it does not exhibit discontinuities in the estimated position but still offers high voltage utilization and a good update rate.

REFERENCES

[1] F. Briz and M. Degner, "Rotor position estimation," *IEEE Ind. Electron. Mag.*, vol. 5, no. 2, pp. 24–36, Jun. 2011. Accessed: Sep. 18, 2020, doi: 10.1109/MIE.2011.941118.

[2] G. Wang, M. Valla, and J. Solsona, "Position sensorless permanent magnet synchronous machine drives—A review," *IEEE Trans. Ind. Electron.*, vol. 67, no. 7, pp. 5830–5842, Jul. 2020. Accessed: Mar. 30, 2020, doi: 10.1109/TIE.2019.2955409.

[3] J. Holtz and H. Pan, "Elimination of saturation effects in sensorless position controlled induction motors," presented at the IEEE Ind. Appl. Conf. 37th IAS Annu. Meeting, Oct. 2002, doi: 10.1109/IAS.2002. 1043762.

[4] P. Landsmann, "Anisotropie-basierte Schätzung der Rotorlage," in *Elektrische Antriebe— Regelung von Antriebssystemen*, 4th ed., D. Schröder, Ed. Berlin, Germany: Springer, 2015, ch. 15, pp. 943–984.

[5] M. Schroedl, "Sensorless control of AC machines at low speed and standstill based on the 'INFORM' method," presented at the IEEE Ind. Appl. Conf. 31st IAS Annu. Meeting, Oct. 1996, doi: 10.1109/IAS.1996.557028.

[6] E. Robeischl and M. Schroedl, "Direct axis current utilization for intelligent sensorless permanent magnet synchronous drives," presented at the IEEE Ind. Appl. Conf. 36th IAS Annu. Meeting, Sep. 2001, doi: 10.1109/IAS.2001.955463.

[7] P. Landsmann, "Sensorless control of synchronous machines by linear approximation of oversampled current," Ph.D. dissertation, Dept. Elect. Comput. Eng., Technische Universität München, Munich, Germany, 2014.

[8] J. Jiang and J. Holtz, "Accurate estimation of rotor position and speed of induction motors near standstill," presented at the 2nd Int. Conf. Power Electron. Drive Syst., May 1997, doi: 10.1109/PEDS.1997.618623.

[9] J. Jiang, *Drehgeberlose Feldorientierte Regelung für Asynchronmaschinen bei Ständerfrequenz Null*. Aachen, Germany: Shaker, 2000.

[10] R. Strothmann, "Device and method for determining the rotational position of a rotor in an electric machine," WO Patent 2007 073 853 A1, Jul. 5, 2007.

[11] C. Mantala, "Sensorless control of brushless permanent magnet motors," Ph.D. dissertation, Dept. Elect. Energy Technol., South Westphalia Univ. Appl. Sci., Soest, Germany, 2013.

[12] Y. Iwaji, R. Takahata, T. Suzuki, and S. Aoyagi, "Position sensorless control method at zero-speed region for permanent magnet synchronous motors using the neutral point voltage of stator windings," *IEEE Trans. Ind. Appl.*, vol. 52, no. 5, pp. 4020–4028, Sep. 2016. Accessed: Sep. 13, 2019, doi: 10.1109/TIA.2016.2582118.

[13] K. Schuhmacher, E. Grasso, and M. Nienhaus, "Improved rotor position determination for a sensorless star-connected PMSM drive using direct flux control," *J. Eng.*, vol. 2019, no. 17, pp. 3749–3753, Jun. 2019. Accessed: Nov. 29, 2019, doi: 10.1049/joe.2018.8055.

[14] T. Werner, *Geberlose Rotorlagebestimmung in Elektrischen Maschinen. Spannungsbasierte Verfahren für Permanentmagneterregte Synchronmotoren*. Wiesbaden, Germany: Springer, 2018, doi: 10.1007/978-3-658-22271-0.

[15] K. Schuhmacher, S. Kleen, and M. Nienhaus, "Comparison of anisotropy signals for sensorless control of star-connected PMSMs," presented at the IEEE 10th Int. Symp. Sensorless Control Electr. Drives (SLED), Sep. 2019, doi: 10.1109/SLED.2019.8896351.

[16] P. Thiemann, C. Mantala, J. Hördler, A. Trautmann, D. Groppe, R. Strothmann, and E. Zhou, "New sensorless rotor position detection technique of PMSM based on direct flux control," presented at the Int. Conf. Power Eng., Energy Electr. Drives (POWERENG), May 2011, doi: 10.1109/PowerEng.2011.6036516.

[17] M. W. Degner and R. D. Lorenz, "Using multiple saliencies for the estimation of flux, position, and velocity in AC machines," *IEEE Trans. Ind. Appl.*, vol. 34, no. 5, pp. 1097–1104, Feb. 1998. Accessed: Feb. 13, 2020, doi: 10.1109/28.720450.

[18] D. Paulus, P. Landsmann, S. Kuehl, and R. Kennel, "Arbitrary injection for permanent magnet synchronous machines with multiple saliencies," presented at the IEEE Trans. Energy Convers. Congr. Expo. (ECCE), Sep. 2013, doi: 10.1109/ECCE.2013.6646744.

[19] M. P. Kazmierkowski, M. Malinowski, and M. Bech, "Pulse width modulation techniques for three-phase voltage source converters," in *Control in Power Electronics: Selected Problems*, M. P. Kazmierkowski, R. Krishnan, and F. Blaabjerg, Eds. New York, NY, USA: Academic, 2002, ch. 4, pp. 89–114.

[20] J. W. Kolar, H. Ertl, and F. C. Zach, "Influence of the modulation method on the conduction and switching losses of a PWM converter system," *IEEE Trans. Ind. Appl.*, vol. 27, no. 6, pp. 1063–1075, Nov. 1991. Accessed: Apr. 17, 2020, doi: 10.1109/28.108456.

[21] J. Holtz and J. Juliet, "Sensorless acquisition of the rotor position angle of induction motors with arbitrary stator windings," *IEEE Trans. Ind. Appl.*, vol. 41, no. 6, pp. 1675–1682, Nov. 2005. Accessed: Apr. 30, 2019, doi: 10.1109/TIA.2005.858245.

[22] D. G. Holmes and T. A. Lipo, *Pulse Width Modulation for Power Converters: Principles and Practice*. Hoboken, NJ, USA: Wiley, 2003.

[23] N. Chernov. (Apr. 21, 2020). *Circle Fit (Pratt Method), MATLAB Central File Exchange*. [Online]. Available: https://de.mathworks.com/matlabcentral/fileexchange/22643-circle-fit-pratt-method

STEPHAN KLEEN was born in Sande, Germany, in 1972. He studied precision engineering with the University of Applied Sciences, Wilhelmshaven, and the mechatronics with the Saarland University. His professional career started with the Mainz Institute of Microtechnology, Mainz. He was the Co-Founder and Technical Director with mymotors and actuators GmbH, the Group Leader Microsystems with Dr. Fritz Faulhaber GmbH & Company KG, a Doctoral Researcher with Saarland University, and the Technical Director with Wellgo Systems GmbH. His research interest includes the design and optimization of electromagnetic drive systems with focus on the sensorless operation of PMSMs.

CHRIS MAY was born in Manila, Philippines, in 1967. He received the B.S. degree in mechanical engineering from the University of New Mexico, Albuquerque, in 1991. From 1993 to 2012, he researched and developed unconventional field-controlled actuators with the Laboratory of Process Automation, Saarland University, Germany. During this time, he made defining contributions, including scientific coordination to numerous European supported collaborative RTD projects investigating the application potential of magnetostrictive and other actuation technologies in aeronautic and robotic structures. Since 2012, he has been a Scientific Assistant with the Laboratory of Actuation Technology, where he contributing to the ongoing research in the field of low-power electrical machines.

KLAUS SCHUHMACHER was born in Trier, Germany, in April 1991. He received the B.Sc. and M.Sc. degrees in mechatronics from the Saarland University, Saarbrücken, Germany, in 2014 and 2016, respectively. From 2014 to 2016, he worked as a Research Assistant with the Laboratory of Actuation Technology, where he became a Doctoral Researcher, in July 2016. His research interests include sensorless control of PMSMs and embedded drive systems.

MATTHIAS NIENHAUS was born in July 1963. He studied precision engineering with the Fachhochschule Furtwangen and electrical engineering with the University of Erlangen-Nürnberg, Germany. He received the Ph.D. degree from the Institute for Microtechnology Mainz (IMM), Germany, in 1998. His professional carrier led him the Head of Precision Engineering Department, Bosch, Siemens, and IMM. He was the Shareholder and the Managing Director of mymotors & actuators GmbH and the Area Director Microsystems of Faulhaber. He is currently a Full Professor with the Saarland University and the Head of the Laboratory of Actuation Technology (LAT), where he teaches and conducts research in the field of small and micro electromagnetic drives with main focus on embedded drive systems and sensorless control processes. Moreover, he leads research activities in the field of electromagnetic motor design and technology for efficient low-power mechatronic devices and systems.